

**This is the author version of article published as:**

Narayanan, S. and Mahendran, Mahen (2003) Ultimate Capacity of Innovative Cold-formed Steel Columns. *Journal of Constructional Steel Research* 59(4):pp. 489-508.

Copyright 2003 Elsevier

## Ultimate Capacity of Innovative Cold-formed Steel Columns

By S. Narayanan<sup>1</sup> and M. Mahendran<sup>2</sup>

### ABSTRACT

This paper describes the distortional buckling behaviour of a series of innovative cold-formed steel columns. More than 15 laboratory experiments were undertaken first on these innovative steel columns of intermediate length under axial compression. All of these columns failed by distortional buckling with very little post-buckling strength. The section and buckling properties of the columns were determined using the finite strip analysis program THINWALL. The distortional buckling and nonlinear ultimate strength behaviour of the columns was investigated in detail using finite element analyses (ABAQUS). The finite element analyses included relevant geometric imperfections and residual stresses. The deflection and strain results from the experiments compared well with those from the analyses. The ultimate design load capacities were evaluated using the provisions of Australian Cold-formed Steel Structures Standard AS/NZS 4600-1996, and were compared with those from experiments and finite element analyses. A series of parametric studies was also carried out by varying the yield strength, thickness and column length. Details of this investigation and the results are presented in this paper.

1 – Visiting Academic, 2- Associate Professor of Civil Engineering, and Director,  
Physical Infrastructure Centre, School of Civil Engineering, Queensland University of  
Technology, Brisbane, QLD 4000, Australia

# **1 INTRODUCTION**

The use of cold-formed steel structures has increased rapidly in recent times due to significant improvements to manufacturing technologies and development of thin, high strength steels. The nominal yield strength of available steels ranges from 250 to 550 MPa while thicknesses less than 1 mm are commonly used. Cold-formed steel sections have distinct structural stability problems, which are not observed in hot-rolled steel sections. In steel compression members, three structural instability modes, namely local, distortional and flexural / flexural – torsional buckling, are likely to occur. Distortional buckling usually occurs in the flanges of channel or other sections if the lip stiffener is inadequate to prevent its movement normal to the plane of the flange it supports.

In the past, researchers have investigated the various buckling modes of commonly used cold-formed steel sections. Hancock [1] presented a detailed study of a range of buckling modes (local, distortional and flexural-torsional) in lipped channel sections. He showed that the distortional mode of buckling may control the design for certain geometries, especially those with rear flanges or lipped rear flanges. Lau and Hancock [2] provided simple analytical expressions to allow the distortional buckling stress to be calculated explicitly for any geometry of cross-section of thin-walled lipped channel section columns. Lau and Hancock [3] provided design curves for sections where the distortional buckling stress and yield stress were approximately equal. In these cases the failure occurred before the elastic distortional buckling stress was reached. The expressions derived by Lau and Hancock are now included in the Australian cold-formed steel structures code AS/NZS 4600 [4].

Kwon and Hancock [5] studied simple lipped channels and a lipped channel with intermediate stiffener under fixed boundary conditions. They chose section geometry

and yield strength of steel to ensure that a substantial post buckling strength reserve occurs in the distortional mode for the test section.

Davies and Jiang [6] used the Generalised Beam Theory (GBT) to analyse the individual buckling modes either separately or in selected combinations. The GBT allows explicit expressions to be derived for the critical stress and wavelength for distortional buckling. Davies and Jiang [6] have used the GBT method in distortional buckling analyses and shown that the time required is only a small fraction of the time needed by the finite element or finite strip methods.

Kesti and Davies [7] assessed the applicability of Eurocode 3 [8] to the prediction of the minimum elastic distortional buckling stress in compression of short fixed ended columns with different cross-sections (C-, Hat- and Rack upright sections). The method given in Eurocode 3 does not correlate as well as Lau and Hancock's [2] method with the results given by GBT.

Past developments have aimed at deriving simpler calculation procedures using manual calculations or spreadsheet [9]. This is however difficult as some aspects of behaviour of cold-formed steel sections are very complex. The THINWALL computer program developed by Papangelis and Hancock [10] can be used to investigate local, distortional and flexural-torsional buckling modes [11]. The semi-analytical finite strip method restricts the analysis to simply supported end boundary conditions and a single buckle half-wavelength. Kwon and Hancock [12] developed a nonlinear elastic analysis based on the spline finite strip method that can handle local, distortional and overall buckling modes in the post buckling range and the interactions between them. This method allows for geometric imperfections, arbitrary loading and non-simple boundary conditions.

It is thus noted that local buckling and flexural / flexural- torsional buckling behaviour of cold-formed steel sections have been extensively studied in the past. In recent times, it has been extended to distortional buckling. However, no studies have been reported on distortional buckling behaviour of compression members with complex geometries. This paper describes the details of such a study.

This study is part of a design project of civil engineering undergraduate students at Queensland University of Technology (QUT) who were asked to design innovative and economical open cold-formed steel column sections of 1000 mm length to resist an axial compression load of 100 kN. The innovation was measured in terms of structural efficiency and aesthetics. In designing the innovative and structurally efficient cold-formed steel column sections, the principles followed were (1) Keeping the column slenderness value ( $l/r$ ) as small as possible to increase the overall buckling strength (2) Keeping the plate slenderness value ( $b/t$ ) within limits to eliminate local buckling. This led to innovative columns that are unlikely to buckle locally (form factors closer to 1) or globally (low  $l/r$  values). A total of 16 innovative steel columns designed by the students were made using a press-braking process, and then tested to failure at QUT's Structures Laboratory. The buckling and ultimate strength behaviour of columns was investigated using finite strip and finite element programs, and the results were compared with experimental results and AS/NZS 4600 predictions.

## **2 EXPERIMENTAL STUDY**

The 16 innovative 1000 mm long column sections were made of 0.8 mm and 0.95 mm G550 steel and 0.96 mm and 1.14 mm G250 steel. The cross-sections of the steel columns and their properties are shown in Figure 1 and Table 1, respectively. Column 1 was also tested in lengths of 876 mm, 675 mm, 475 mm, 275 mm, 130 mm and 100 mm. The steel column sections were placed between the cross-heads of a compression testing machine and loaded to failure. The test set-up is shown in Figure 2. The ultimate loads and the nature of failure were noted (Table 4). For the purpose of validation of numerical models, the axial deformations and strains at mid-height for the locations shown in Figure 3 were measured. The failures of all the columns were found to be associated with distortional buckling except for the 130 mm and 100 mm columns, which failed in local buckling.

Most of the columns tested are innovative and practical while some may not be considered practical. Based on the experimental ultimate strength to weight ratios, Column 8 was found to be the most efficient section. As anticipated, columns made of

higher grade steel (G550) were more efficient than those made of lower grade steel (G250).

### 3 FINITE ELEMENT ANALYSIS

Finite element analysis (FEA) of the same 16 innovative steel columns tested to failure in the laboratory was undertaken using ABAQUS [13] and PATRAN. Four-noded, 3-D quadrilateral shell elements (S4R5) were used in the finite element analyses. The measured base metal thicknesses and yield stresses of steels given in Tables 1 and 2 were used. The value of Young's Modulus was taken as 210,000 MPa. A linear elastic buckling analysis was performed first to obtain the buckling loads and associated buckling modes. This was followed by a non-linear ultimate strength analysis to predict the ultimate load capacity. In the latter analysis, elastic-perfectly-plastic material properties were assumed for all steel grades. Following a series of convergence studies, a mesh size of 5 mm x 5 mm was found to be appropriate for the column length of 1000 mm. However, different mesh sizes were also used. For example, to validate the model using the results from the finite strip buckling analysis program THINWALL, shorter length columns were modelled. In this case, 1 mm x 1 mm mesh size was used. The node restraints are specified by the numbers of corresponding degrees of freedom at the node. For example, BC123456 denotes restraints on all 6 degrees of freedom at the node. The influence of rounded corners with internal radius  $r \leq 5t$  and  $r \leq 0.15w$  on section properties can be neglected based on Clause 3 of ENV 1993-1-3 (1996). In this case,  $r \leq 5 \times 0.8 = 4$  mm,  $0.15 \times 20 = 3$  mm, and hence the cross-section was assumed to consist of plane elements with sharp corners.

The structural behaviour of columns under axial compression was modelled using four different types of finite element models. They are briefly described as follows:

Model 1: Full length model, in which the full length of the column was modelled with ends modelled using multi-point constraints (MPC) (BC126 at the top and BC1236 at the base) (Figure 4). The MPCs were considered to model the end conditions of the columns tested. Alternatively, a half length model was used with MPC at the top (BC126) and symmetry conditions at mid-length (BC345).

Model 2: Full length model with the cross-head of the compression testing machine being modelled as a rigid surface at the ends of the column (referred to as rigid body model). The rigid surface was modelled using rigid body elements (R3D4). The reference node for the rigid surface was located at the centroid of the surface and had BC126 at the top and BC1236 at the base (Figure 5). Alternatively, a half length model was used with R3D4 elements at the top (BC126) and symmetry conditions at mid-length (BC345).

Model 3: Half wavelength model based on the half wave buckling length of the column. The ends were modelled using MPC.

Model 4: Half wavelength model based on the half wave buckling length of the column. The ends were modelled using a rigid surface using R3D4 elements.

Detailed investigations showed that both the MPC and rigid body models (Models 1 and 2) were suitable for modelling global buckling behaviour of compression members. Figure 6a shows how the MPC and rigid surface rotate as a plane surface at the ends simulating pinned end conditions. Hence both the above types are also suitable for modelling half wavelength models for global buckling.

The rigid body models (Models 2 and 4) were found to be suitable for local buckling behaviour of compression members as shown in Figure 6b. However, the MPC model was found to be unsuitable for modelling local buckling behaviour due to additional restraints caused by MPC.

It was seen that both MPC and rigid body elements in Models 1 and 2 simulated the actual test conditions for distortional buckling behaviour. The cross-heads of the testing machine offered restraint against lateral movement of the column ends. This restraint against opening out of the lips at the ends was provided by the MPC and rigid body elements. Hence they were suitable for the full and half length experimental models (Models 1 and 2). However, they were not suitable when half-wavelength models (Models 3 and 4) are used for distortional buckling mode. The MPC and rigid body elements were also not suitable with half wavelength models in modelling mixed buckling modes (flexural – torsional and local –distortional buckling modes).

The results obtained using the different finite element models are compared with the distortional buckling loads from THINWALL and the ultimate loads from tests for Column 1 in Table 3. The buckling results from THINWALL are shown in Figure 7.

The elastic critical stress for local buckling of plate elements is given by

$$f = \frac{k\pi^2 E}{12(1-\nu^2)} \left( \frac{t}{w} \right)^2 \quad (1)$$

where  $k = 4.0$  for simply supported plates,  $E$  = Young's modulus,  $\nu$  = Poisson's ratio,  $t$  = thickness of the element and  $w$  = width of the plate element.

The critical local buckling stress determined using Equation 1 for the most slender plate element of Column 1 is 1215 MPa. This local buckling stress is lower than the result from the finite strip analysis program THINWALL (1284 MPa from point A on Figure 7) as it considers the restraints provided by the adjacent plates. The finite strip analysis results in Figure 7 showed that Column 1 buckles distortionally for half wavelengths from about 60 mm to 1200 mm. Local buckling occurs for half wavelengths less than 60 mm whereas overall flexural buckling occurs for half wavelengths greater than 1200 mm. The FEA using Models 1 and 2 of 1000 mm long Column 1 gave distortional buckling stress results that agreed well with the buckling stress from Figure 7 corresponding to the half wavelength observed in the finite element models (see Figure 8 and Table 3). The half wavelength, allowing for the restraints, can be obtained from the deflected shape of the model.

Following the use of four different types of finite element models in which Models 1 and 2 gave very close results (Table 3), it was then decided to use half length models with MPC (Model 1) to simulate the distortional buckling behaviour of all the 16 columns observed in the tests. Elastic distortional buckling loads from these FEA compared well with THINWALL predictions as shown later in Table 5.

In the nonlinear analysis, initial geometric imperfections were modelled by providing initial out-of-plane deflections to the model. The first elastic buckling mode shape was used to create the geometric imperfections for the non-linear analysis. The maximum

amplitude of the buckled shape determined the degree of imperfection. For distortional buckling modes, the imperfection was specified in terms of thickness. The maximum value of distortional imperfection was initially taken as approximately equal to the plate thickness  $t$  as recommended by Schafer and Pekoz [14]. Kwon and Hancock [5] found that the geometric imperfections of press-braked 1.2 mm G500 lipped channel columns were in the range of -1.5 mm to 1.0 mm (distortional) and -0.5 to 0.5 mm (overall). These confirm Schaefer and Pekoz's [14] recommendation for distortional imperfection, however, in this study two geometric imperfection magnitudes,  $t$  and  $2t$ , were included to investigate the effects of such imperfections. Kwon and Hancock [5] found that the overall imperfections had little effect on the buckling of the columns of intermediate length since these columns generally buckled in a local, distortional or mixed mode of local and distortional buckling. This study therefore did not include any overall imperfections in the FEA.

Modelling imperfections for local buckling was undertaken by using imperfection values of  $\frac{w}{167}$  by Schafer and Pekoz [14]. To study the effect of variations in imperfections on the ultimate load, imperfection magnitudes of  $\frac{w}{167}$  and  $\frac{2w}{167}$  were used in the nonlinear analyses. These values of imperfections are comparable with the upper limit recommended by the BS 5950 formula [15]:

$$\frac{\delta_c}{t} = 0.145 \left( \frac{w}{t} \right) \sqrt{\frac{f_y}{E}} \quad (2)$$

where

$\delta_c$  = Imperfection value

$t$  = thickness of the member

$w$  = width of a plate element of the member

$f_y$  = Yield strength of the material

$E$  = Young's modulus

For a 20 mm wide plate with 0.8 mm thickness, this value is 0.2 mm using Equation 2 as against the values of 0.12 mm ( $\frac{w}{167}$ ) and 0.24 mm ( $\frac{2w}{167}$ ) used in this study.



The plot of the ratio of the non-linear ultimate load (with zero imperfection) to the buckling load for each column versus the square root of the ratio of yield stress to the buckling stress is shown in Figure 9. From the figure it can be seen that as the slenderness (i.e. square root of the ratio of the yield stress to the buckling stress) increases, the post buckling strength increases. This agrees well with the observations made by Lau and Hancock [3] for channel section columns.

The residual stresses have also been included in the nonlinear analyses although their effect on the ultimate load is considered small [14]. In cold-formed steel members, residual stresses are dominated by flexural or through the thickness variation of stresses. These residual stresses lead to early yielding on the faces of steel plates. Residual stresses are idealised into flexural and membrane stresses. Membrane stresses are more prevalent in roll-formed members than press-braked members. Flexural residual stresses of up to 50% yield stress ( $f_y$ ) have been observed [14]. However, both these values are highly variable. The average residual stress distribution recommended by Schafer and Pekoz [14] for a press-braked lipped C-section is shown in Figure 10.

For this study an average flexural residual stress value of 17%  $f_y$  has been applied uniformly to all the plate elements of the columns. The variation of flexural residual stress through the thickness was assumed to be linear with zero stress at the centre. It is assumed that the higher residual stress at the corners is compensated by the increased yield strength at the same location. Since the membrane residual stress is significantly less than the flexural residual stress, the former has been ignored.

The residual stresses were modelled using the ABAQUS \*INITIAL CONDITIONS option with TYPE=STRESS, USER. The user defined initial stresses were created using the SIGINI Fortran user subroutine. It was ensured that the residual stresses were correctly defined with tension on the outside faces and compression on the inside faces. The initial stresses were applied in a \* STATIC step with no loading and the standard model boundary conditions to allow equilibration of the initial stress field before starting the response history. Table 4 compares the FEA ultimate load capacities of the columns with and without residual stresses with the test ultimate load.

## 4 COMPARISON OF EXPERIMENTAL AND FEA RESULTS

Table 4 shows that the finite element models give good predictions of the ultimate loads of the columns tested. When the imperfection magnitude was assumed equal to the plate thickness  $t$ , the FEA predictions were on average about 6% higher than the test loads (mean of 1.06) with a COV of 0.127 and a maximum error of 28% (overpredicts). The use of an imperfection of  $2t$  gave lower ultimate loads with a mean of 0.972 and COV of 0.142 (without residual stresses), but the maximum error was 30% (underpredicts). The table shows that the change in ultimate load produced by the effect of including residual stresses is very small. When imperfection value is  $t$ , the addition of residual stresses improved the prediction by lowering the mean value to 1.034 with a COV of 0.117. The maximum overprediction is 28% and maximum underprediction is 16%. For the imperfection value of  $2t$ , when residual stresses are also included, the corresponding values are 0.956, 0.128 and 30%. Some sections appear to be more sensitive to imperfections than others, for example, the ultimate capacity of Column 6 reduces drastically on application of imperfection, from 139.8 kN to 78.2 kN (for imperfection  $t$ ) and 66.6 kN (for imperfection  $2t$ ). Similarly, Column 15 is also seen to be sensitive to imperfections. These observations clearly show that cold-formed steel columns with certain geometries will be very sensitive to geometrical imperfections and thus demonstrate the need to include appropriate geometrical imperfection magnitudes in FEA. It is noted that except for Column 1, FEA using a geometrical imperfection of  $t$  gives good comparisons with test results. From these observations, it can be concluded that using a maximum distortional imperfection value of  $t$  as recommended by Schafer and Pekoz [14] appears to be satisfactory.

Figure 11 compares the axial compression load versus shortening curves of the test and FEA for Column 1 whereas Figure 12 compares the test and FEA strain curves. These curves show reasonably good agreement between the test and FEA results.

## 5 DESIGN CODE PREDICTIONS

AS/NZS 4600 (SA, 1996) includes provisions for distortional buckling that are based on research including testing of rack and C-sections by Lau and Hancock [3] and Kwon

and Hancock [12]. Nominal member capacity ( $N_c$ ) of the sections subjected to distortional buckling is given by:

$$N_c = Af_y \left[ 1 - \frac{f_y}{4f_{od}} \right] \quad \text{when } f_{od} > \frac{f_y}{2} \quad (3)$$

$$N_c = Af_y \left[ 0.055 \left( \sqrt{\frac{f_y}{f_{od}}} - 3.6 \right)^2 + 0.237 \right] \quad \text{when } \frac{f_y}{13} \leq f_{od} \leq \frac{f_y}{2} \quad (4)$$

where  $A$  = gross area,  $f_y$  = yield stress,  $f_{od}$  = elastic distortional buckling stress,

The member capacities (or ultimate load) based on distortional buckling were calculated using Equations 3 and 4 for all the test columns and are given in Table 5. For G550 steel columns with less than 0.9 mm thickness, 75%  $f_y$  was used in the capacity calculations as recommended by AS/NZS 4600.

Table 5 also includes the buckling loads predicted by the FEA and THINWALL as the corresponding distortional buckling stress ( $f_{od}$ ) was used in the AS/NZS 4600 ultimate load calculations. Comparison of FEA and test ultimate loads with AS/NZS 4600 predictions in Table 5 shows that AS/NZS 4600 over-predicts the ultimate loads by up to 32% and 12% for G550 and G250 steel columns whereas it under-predicts the ultimate loads by up to 1% and 15% for the same columns. When 0.75  $f_y$  was used in the calculations for 0.8 mm G550 steel columns, the predictions were improved, giving an average ratio of 1.061 and a COV of 0.121. This observation justifies the use of AS/NZS 4600 rule of using 0.75  $f_y$  for G550 steels with less than 0.9 mm thickness. It is also seen that the mean ratio of AS/NZS 4600 ultimate load to the FEA ultimate load (with residual stresses and imperfection value of  $t$ ) improved from 1.088 (with COV of 0.109) to 1.033 (with COV of 0.131) when 0.75 $f_y$  was used. However, this rule was not used for 0.95 mm G550 steel columns, and in this case the code over-predicted the ultimate load by up to 32% (see Table 5). There were also other cases when over-prediction of more than 20% occurred. This might have been either due to the inadequacy of using 0.75 $f_y$  for G550 steels or of the design equations in predicting ultimate strengths for distortional buckling. Further experimental and numerical research is needed to improve this.

## 6 PARAMETRIC STUDIES

A series of parametric studies was also undertaken for one of the columns (Column 1). Since the effect of residual stresses on the ultimate loads was found to be small in most cases (less than 5% in Table 4), the FEA in the parametric studies did not include any residual stresses. The thickness  $t$  was varied from 0.6 mm to 2.0 mm and the yield strength  $f_y$  was varied from 250 MPa to 1500 MPa while keeping the length the same at 1000 mm. The ultimate loads increased substantially for yield strengths up to 750 MPa after which the increase in ultimate load capacity was negligible. The ultimate loads increased rapidly as the thickness was increased. The parametric study results also indicated the lack of post buckling strength for all values of  $f_y$  and thickness.

The parametric studies also considered a series of different lengths (1000 mm, 876 mm, 675 mm, 475 mm, 275 mm, 130 mm and 100 mm) for Column 1. To further validate the numerical results, they were also tested to failure. The FEA results are compared with the test results in Table 6. The test ultimate loads are also compared with AS/NZS 4600 predictions in Table 6. Comparison of test ultimate loads with FEA ultimate loads and AS/NZS 4600 predictions in Table 6 gave similar ratios to those obtained earlier from Tables 4 and 5. Table 6 results also showed that AS/NZS 4600 over-predicts the ultimate loads for the G550 steel columns, however, when  $0.75 f_y$  was used in the calculations, the predictions were improved. This observation further justifies the use of AS/NZS 4600 rule of using  $0.75 f_y$  for G550 steels with less than 0.9 mm thickness. However, further experimental and numerical research is needed to improve the accuracy of design code predictions for distortional buckling strengths of innovative cold-formed steel columns made of thin, high strength steels.

Further details of this study including experimental, numerical and parametric studies and the results are given in Narayanan and Mahendran [16].

## 7 CONCLUSIONS

This paper has described an investigation into the buckling and ultimate strength behaviour of a series of innovative cold-formed steel members subject to axial

compression. Both laboratory experiments and numerical analyses were used to study their structural behaviour dominated by distortional buckling. Effects of geometrical imperfections and residual stresses on the ultimate load were investigated. It was found that residual stresses had only a very small effect on the ultimate load. The ultimate strength results from experiments, finite element analyses and the design standard were compared, and appropriate recommendations were made. A series of parametric studies was also carried out by varying the yield strength, thickness and length of columns, and these results are also included in this paper. This investigation has shown that further research is needed to improve the accuracy of design code predictions for distortional buckling strengths of innovative cold-formed steel columns made of thin, high strength steels.

## **8 ACKNOWLEDGEMENTS**

The authors wish to thank the Physical Infrastructure Centre and the School of Civil Engineering at Queensland University of Technology for providing the required facilities and technical support for this research project. They also wish to thank the TKM College of Engineering of the Kerala University and the Faculty of Built Environment and Engineering, QUT for supporting the first author's study leave program at QUT during 2001.

## **References**

- [1] Hancock GJ. Distortional buckling of steel storage rack columns. *J Struct Engng*, 1985;111(12): 2770-2783.
- [2] Lau SCW, Hancock GJ. Distortional buckling formulas for channel columns. *J Struct Engng*, ASCE 1987; 113(5): 1063-1078.
- [3] Lau SCW, Hancock GJ. Inelastic buckling of channel columns in the distortional mode. *Thin-Walled Struct J* 1990; 59-84.
- [4] Standards Australia (SA), Australian/ New Zealand Standard AS/NZS 4600. Cold formed steel structures, Sydney. 1996.
- [5] Kwon YB, Hancock GJ. Tests of cold-formed channels with local and distortional buckling. *ASCE J of Struct Engng*. 1992, 117(7):1786-1803.

- [6] Davies JM, Jiang C. Design for distortional buckling. *J Construct Steel Res.* 1998,46:174-175.
- [7] Kesti J, Davies JM. Local and distortional buckling of thin-walled short columns. *Thin-Walled Struct.* 1999,34: 115-134.
- [8] ENV 1993-1-3:1996/AC European Pre-standard Design of Steel Structures-Part 1-3: General rules - Supplementary rules for cold formed thin gauge members and sheeting,1996.
- [9] Davies JM. Modelling, analysis and design of thin-walled steel structures. *Light-Weight Steel and Aluminium Structures*, (P.Makelainen and P.Hassinen, editors), Elsevier Science Ltd. 1999.
- [10] Papangelis JP, Hancock GJ. Computer analysis of thin-walled structural members. *Computers and Structures.* 1995,56, 1, 157 – 176.
- [11] University of Sydney, THIN-WALL - Users Manual. 1996.
- [12] Kwon YB, Hancock GJ. A nonlinear elastic spline finite strip analysis for thin-walled sections. *Thin-Walled Struct.* 1991,12:295-319.
- [13] HKS, Introduction to ABAQUS/ Standard, USA, Hibbitt, Karlsson & Sorenson, Inc. 1998.
- [14] Schafer BW, Pekoz T. Computational modelling of cold-formed steel: characterizing geometric imperfections and residual stresses. *J Construct Steel Res.* 1998,47: 193-210.
- [15] British Standards Institution (BSI), BS 5950-5, Structural use of steel work in building - Code of Practice for design of cold formed thin gauge sections. 1998.
- [16] Narayanan S, Mahendran M. Ultimate capacity of innovative cold-formed steel columns. Research Monograph 2001-6, Physical Infrastructure Centre, Queensland University of Technology, Brisbane. 2001.

Column 1	Column 2	Column 3	Column 4
Column 5	Column 6	Column 7	Column 8
Column 9	Column 10	Column 11	Column 12
Column 13	Column 14	Column 15	Column 16

**Figure 1. Section geometries of the innovative steel columns**  
(All dimensions are measured values in mm)



**Figure 2. Test set up**

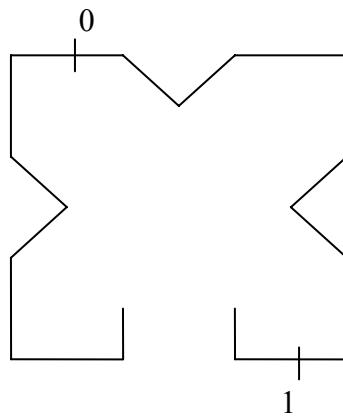


**Figure 3. Locations of strain measurement for Column 1**



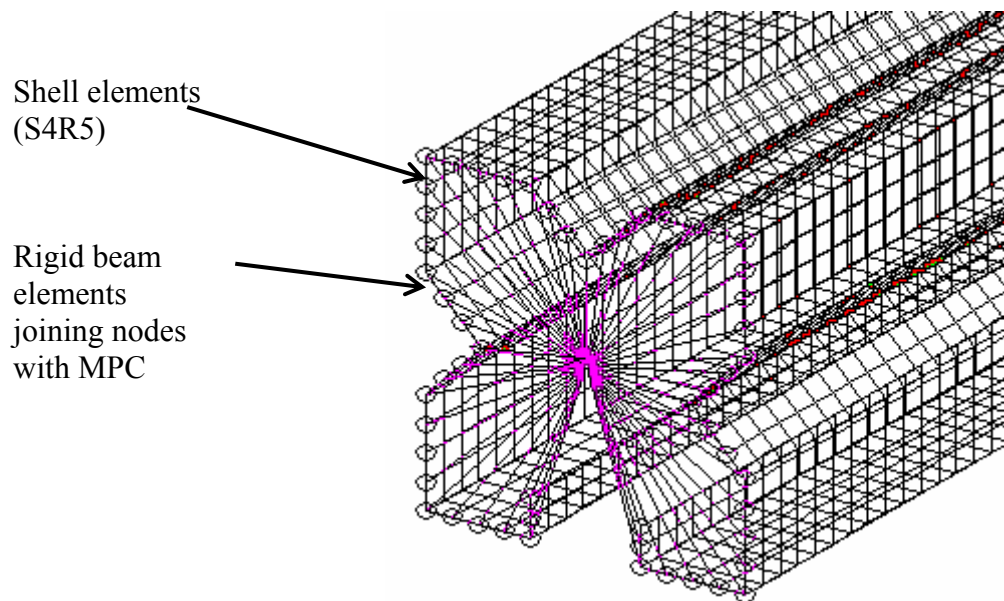


**Figure 4. Column ends modelled using MPC**

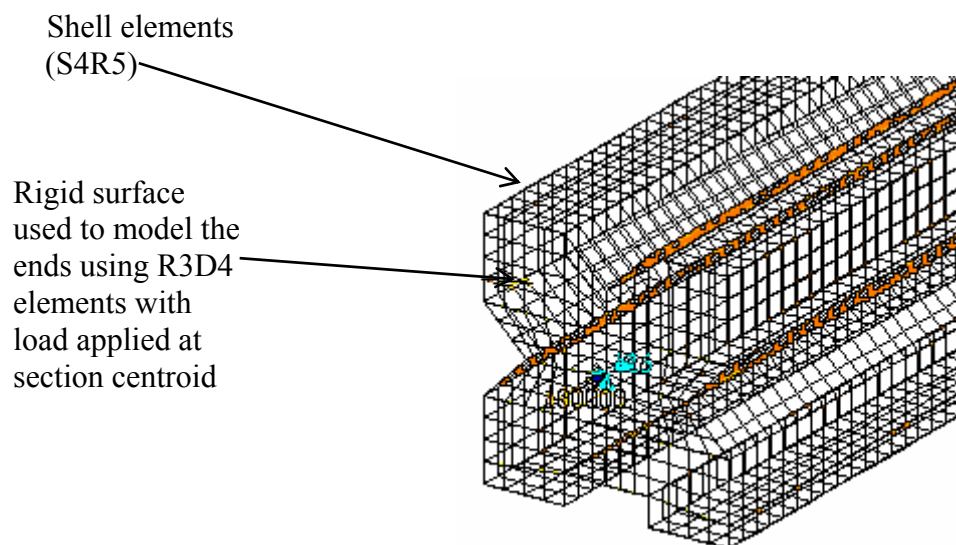


**Figure 5. Column ends modelled using R3D4 elements**

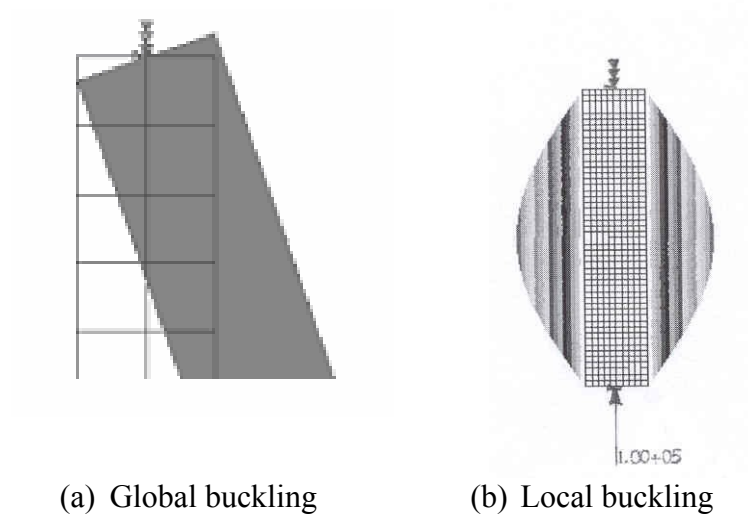


**Figure 6. Use of MPC and rigid body elements in FEA**

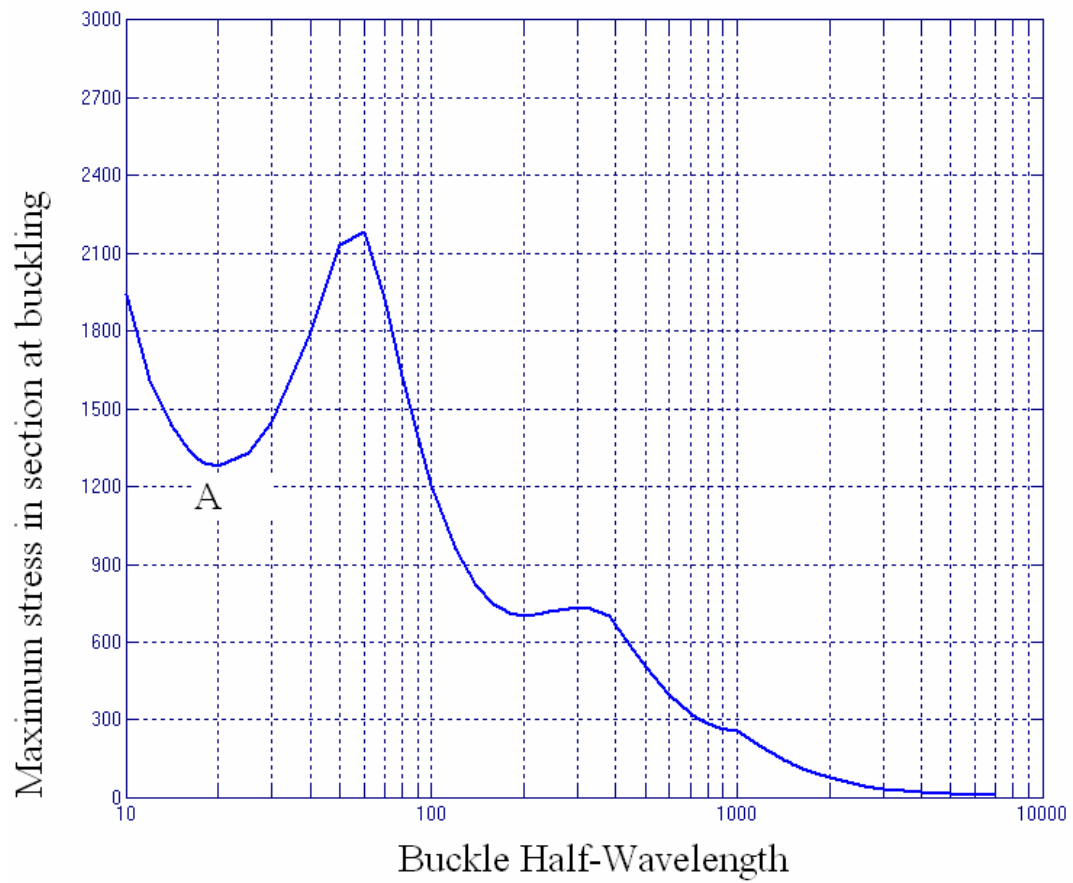


**Figure 7. Buckling plot from THINWALL for Column 1**

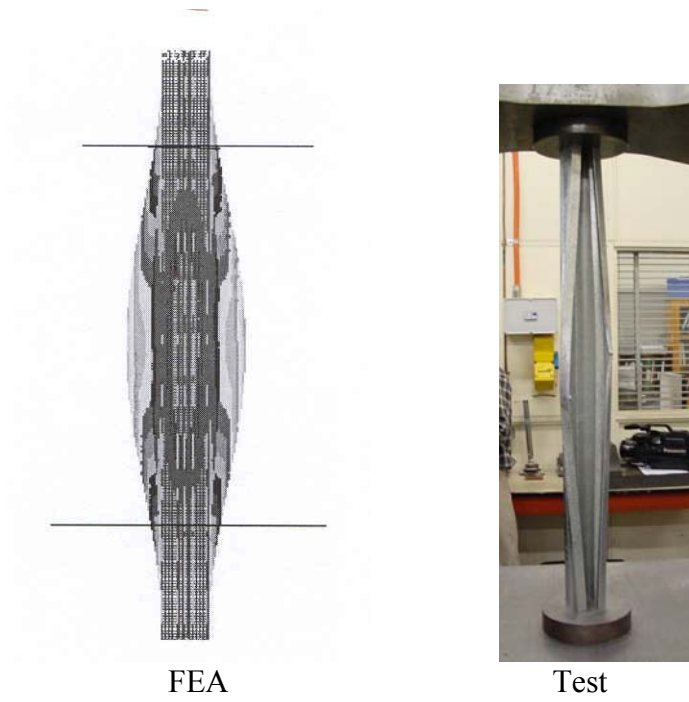


**Figure 8. Distortional buckling of Column 1 from FEA and Test**

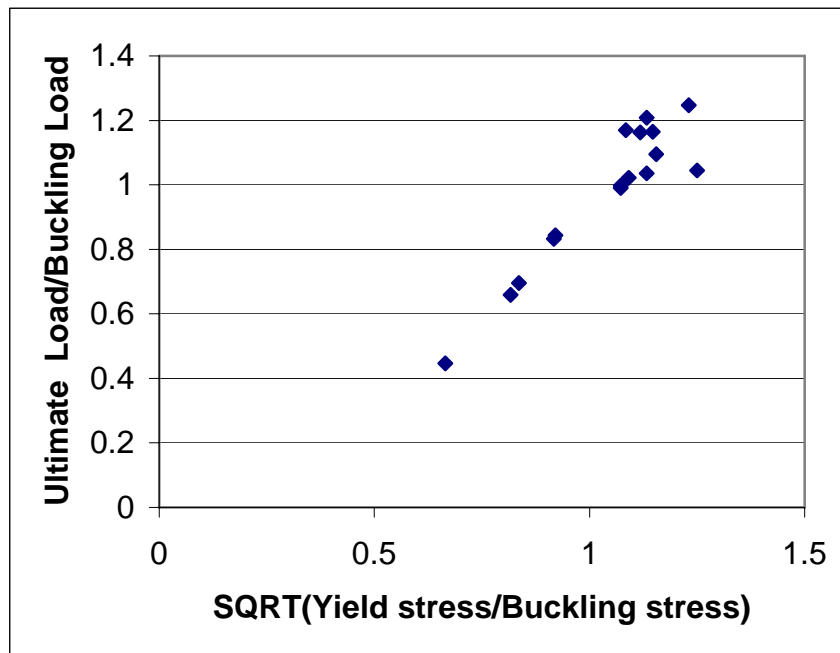


**Figure 9. Plot of Ultimate Load/Buckling Load Vs SQRT (Yield Stress/Buckling Stress)**

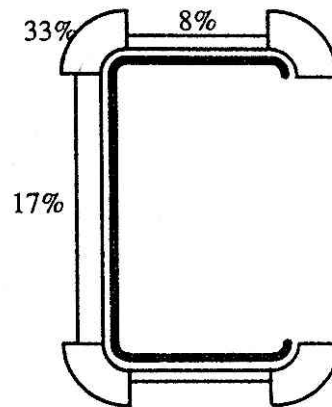


**Figure 10.** Average flexural residual stress as a percentage of  $f_y$  [14]

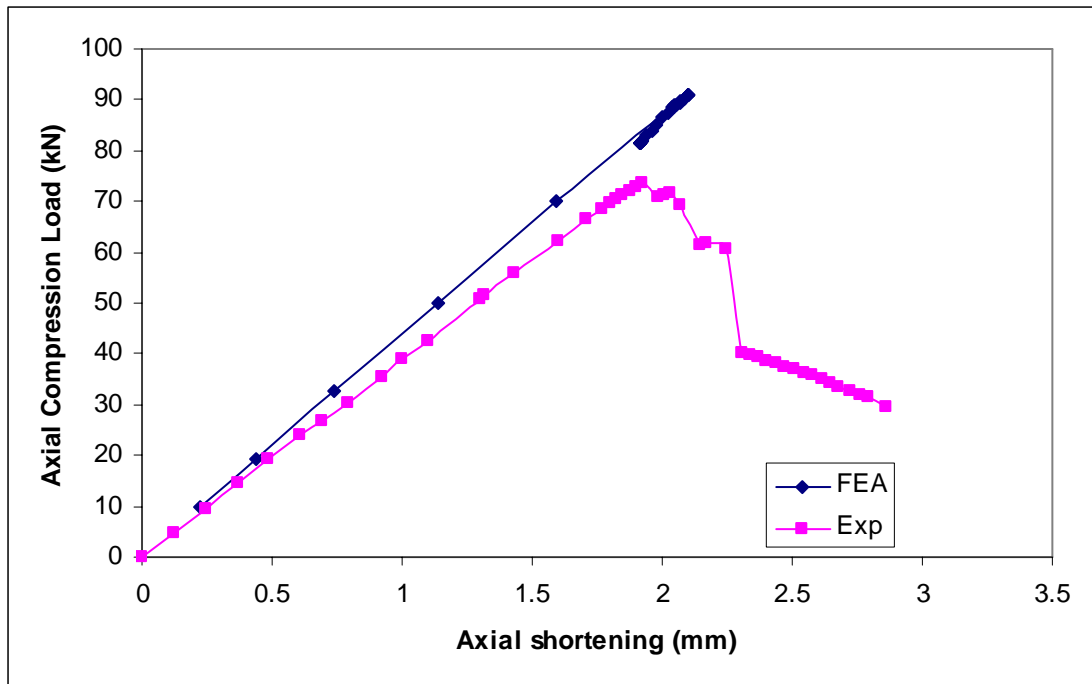
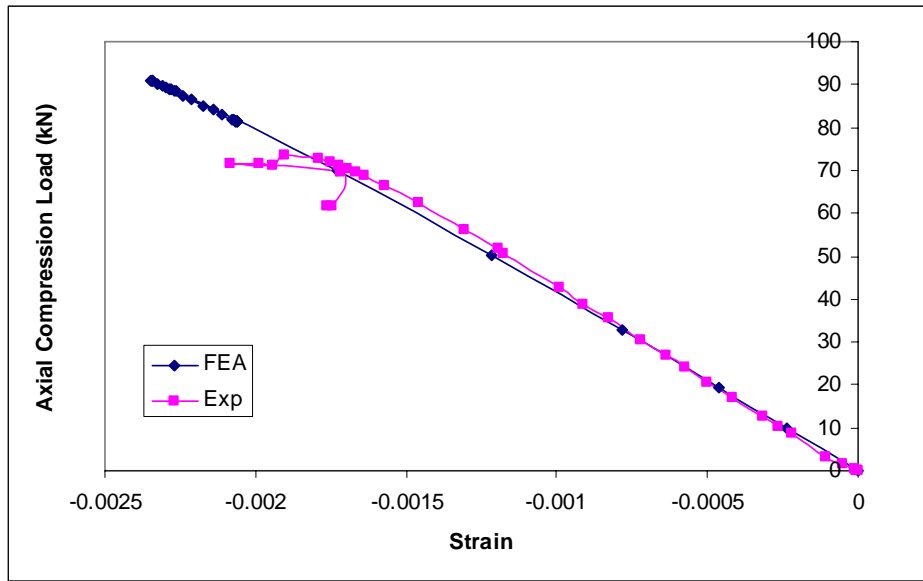
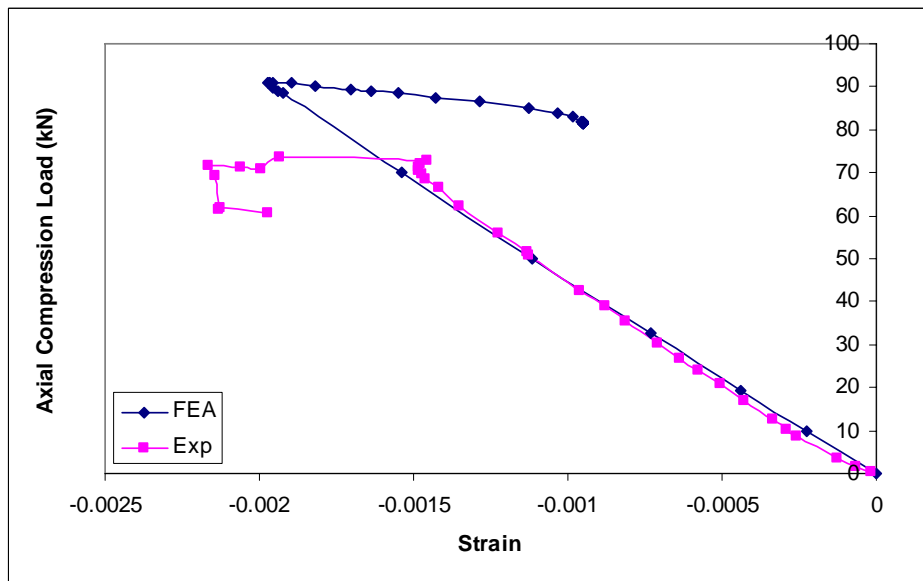


**Figure 11. Axial compression load Vs Shortening curve for Column 1**



(a) Location 0



(b) Location 1

Figure 12. Axial compression load vs Strain curves for Column 1



**Table 1. Properties of steel column sections**

Column Number	Steel Grade	Thickness	Gross area	L/r**
		(mm)*	(mm <sup>2</sup> )	
1	550	0.80	211.2	43.0
2	550	0.80	240.0	45.5
3	550	0.80	212.8	36.9
4	550	0.80	249.6	40.3
5	550	0.80	235.5	39.8
6	550	0.95	247.0	44.4
7	550	0.95	267.0	45.8
8	550	0.95	227.0	53.7
9	550	0.95	245.1	41.7
10	550	0.95	267.9	44.2
11	250	0.96	430.7	30.8
12	250	0.96	405.1	34.6
13	250	0.96	426.3	30.2
14	250	0.96	379.2	39.0
15	250	1.14	362.5	28.6
16	250	1.14	380.9	41.4

Note: \* - Base metal thickness; \*\*L/r = Critical column slenderness ratio

**Table 2. Yield stress of steel**

Grade	Base metal thickness (mm)	Yield Stress (MPa)
G550	0.80	656
	0.95	637
G250	0.96	326
	1.14	310

**Table 3. Comparison of buckling and ultimate loads in kN for Column 1**

Model	Buckling Load**		FEA Ultimate load			Test Ultimate Load
	THINWALL	FEA	zero	t*	2t*	
1	108.6	115.8	118.4	90.8	81.0	78.0
2	108.6	115.7	118.3	90.5	80.8	78.0

\* magnitude of geometric imperfections, \*\* - Distortional Buckling

**Table 4. Comparison of FEA and Test ultimate loads**

Column	Test ultimate load (kN)	FEA ultimate loads (kN)						FEA/ Test ultimate load			
		None**			0.17 f <sub>y</sub> **			None**		0.17 f <sub>y</sub> **	
		zero*	t*	2t*	zero	t*	2t*	t*	2t*	t*	2t*
1	78.0	118.4	100.4	92.0	100.0	99.5	91.0	1.287	1.179	1.276	1.167
2	86.0	148.4	98.2	87.6	123.0	91.1	83.2	1.142	1.019	1.059	0.967
3	78.5	121.2	93.2	81.9	121.0	92.6	82.8	1.187	1.043	1.179	1.055
4	91.5	110.0	90.0	82.8	91.9	89.5	83.0	0.984	0.905	0.978	0.907
5	81.0	127.0	101.4	96.4	114.0	85.9	85.2	1.252	1.190	1.060	1.052
6	80.1	139.8	78.2	66.6	117.0	81.0	69.8	0.976	0.831	1.011	0.871
7	104.5	159.0	112.2	102.0	130.0	110.0	99.9	1.074	0.976	1.052	0.956
8	102.0	143.2	93.5	84.6	113.0	93.8	84.0	0.917	0.829	0.920	0.824
9	89.0	134.0	102.0	93.5	119.0	101.0	92.7	1.146	1.050	1.135	1.042
10	87.5	140.0	96.5	88.2	144.0	96.0	88.2	1.103	1.008	1.097	1.008
11	145.0	139.8	128.0	121.0	134.0	127.0	121.	0.883	0.834	0.876	0.834
12	94.5	107.0	92.9	91.9	93.6	89.1	88.2	0.983	0.972	0.943	0.933
13	100.2	138.0	113.0	109.0	121.0	111.0	108.	1.128	1.088	1.108	1.078
14	115.5	122.0	105.0	97.2	107.0	103.0	97.0	0.909	0.842	0.892	0.840
15	83.1	112.0	70.1	58.1	107.0	69.6	58.0	0.844	0.699	0.836	0.698
16	92.5	117.0	106.0	100.0	111.0	104.0	98.7	1.146	1.081	1.124	1.067
							mean	1.060	0.972	1.034	0.956
							COV	0.127	0.142	0.117	0.128

\* - magnitude of geometric imperfections

\*\* - residual stresses

**Table 5. Comparison of Test and FEA results with design code predictions**

Column	Buckling load (kN)		Test Ult. Load (kN)	AS/NZS 4600 Ult. load (kN)		Ultimate Load AS/NZS 4600/Test		Ultimate Load AS/NZS 4600/FEA(t*)	
	Thin-Wall	Abaqus		$f_y$	$0.75f_y$	$f_y$	$0.75f_{y**}$	$f_y$	$0.75f_{y**}$
1	108.6	115.8	78.0	97.1	80.6	1.25	1.03	0.976	0.810
2	123.1	122.7	86.0	106.9	89.7	1.24	1.04	1.173	0.984
3	117.0	121.6	78.5	99.5	82.2	1.27	1.04	1.075	0.888
4	105.1	105.3	91.5	100.1	87.0	1.09	0.95	1.118	0.972
5	114.9	116.0	81.0	103.1	86.9	1.27	1.07	1.200	1.011
6	126.0	120.0	80.1	105.8		1.32	1.32	1.306	1.306
7	139.6	136.7	104.5	117.2		1.12	1.12	1.065	1.065
8	116.9	122.4	102.0	101.9		0.99	0.99	1.086	1.086
9	134.4	135.4	89.0	111.1		1.25	1.25	1.100	1.100
10	93.6	112.3	87.5	105.8		1.21	1.21	1.102	1.102
11	274.1	313.8	145.0	124.7		0.86	0.86	0.982	0.982
12	99.1	103.3	94.5	89.9		0.95	0.95	1.008	1.008
13	149.5	163.7	100.2	109.5		1.09	1.09	0.986	0.986
14	146.6	146.6	115.5	97.6		0.85	0.85	0.947	0.947
15	169.1	161.0	83.1	92.8		1.12	1.12	1.333	1.333
16	188.2	177.5	92.5	98.4		1.06	1.06	0.947	0.947
					Mean	1.121	1.061	1.088	1.033
					COV	0.133	0.121	0.109	0.131

Note: \* - magnitude of initial geometric imperfections and also includes residual stresses

\*\* -  $0.75 f_y$  or  $f_y$  as applicable

**Table 6. Comparison of buckling and ultimate loads for different lengths of Column 1**

Column Length (mm)	Type of Failure	Model type	Buckling loads (kN)		FEA Ult. Load* (kN)		Test Load (kN)	AS/NZS 4600		FEA (F1) Test load	AS/NZS 4600 Test load	
			Thin-wall	Abaqus	F1	F2		$f_y$	$0.75f_y$		$f_y$	$0.75f_y$
1000	Dist.	MPC	108.6	115.8	99.5	91.0	78.0	97.1	80.6	1.28	1.24	1.03
876	Dist.	MPC	128.7	137.3	109	100	87.6	103.6	84.3	1.24	1.18	0.96
675	Dist.	MPC	151.2	156.1	105	95.9	90.9	107.8	86.6	1.16	1.18	0.95
475	Dist.	MPC	165.3	177.8	113	106	102.1	111.6	88.7	1.11	1.09	0.87
275	Dist.	MPC	205.5	227.2	122	116	107.2	118.1	92.4	1.14	1.10	0.86
130	Local	Rigid	285.2	301.9	130	128	122.0	137.6	103.9	1.07	1.12	0.85
100	Local	Rigid	270.0	300.5	132	129	123.6	137.6	103.9	1.05	1.11	0.84
									mean	1.15	1.15	0.91
									COV	0.07	0.05	0.08

Note: \* - Includes residual stresses of  $0.17f_y$

F1 - magnitude of initial geometric imperfections was  $t$  and  $(\frac{w}{167})$  for distortional and local buckling modes

F2 - magnitude of initial geometrical imperfections was  $2t$  and  $(\frac{2w}{167})$  for distortional and local buckling modes.